Intense Blue Luminescence of 3,4,6-Triphenyl-α-pyrone in the Solid State and Its Electronic Characterization

Keisuke Hirano, Satoshi Minakata, and Mitsuo Komatsu*

Department of Applied Chemistry, Graduate School of Engineering, Osaka University, 565-0871 Suita, Osaka, Japan

Jin Mizuguchi*

Department of Applied Physics, Graduate School of Engineering, Yokohama National University, 240-8501 Yokohama, Japan

Received: October 17, 2001; In Final Form: February 18, 2002

Luminescent and electronic properties of 3,4,6-triphenyl-α-pyrones have been investigated from the standpoints of fluorophore and crystal structures. 3,4,6-Triphenyl-α-pyrones are found to emit intense blue to orange luminescence in the solid state, although the luminescence is quite weak in solution. Among these, **3a** exhibits the strongest blue luminescence peaking around 470 nm with an intensity at least three times stronger than that of Alq_3 (λ_{max} = ca. 530 nm). Therefore, **3a** can possibly be applied as a blue emitter for EL devices. Structurally, **3a** has the characteristics of a dimerlike arrangement in the solid state. Due to excitonic interactions based on this molecular arrangement, the absorption band is found to shift toward longer wavelengths by about 36 nm (about 2933 cm^{-1}) on going from solution to the solid state.

1. Introduction

Electroluminescence (EL) has been the focus of considerable interest because of its high potential for compact and clear display devices.[1] Although a great number of compounds are known which fluoresce in solution, fluorophores in the solid state are relatively limited. In addition, the display application requires the three primary colors of high purity (blue, green, and red). Tris(8-hydroxyquinolino)aluminum (Alq_3) is a well-known, promising green emitter in the solid state, although the intensity in solution is relatively weak.[2] On the other hand, blue and red emitters are less than ideal at the moment. Some attempts have been made to achieve blue emitters in metal complexes based on the 8-hydroxyquinoline derivatives. For example, lithium tetra(2-methyl-8-hydroxy-quinolate) boron and bis(2-methyl-8-quinolinolate) aluminum(III) hydroxide have been found to be efficient, blue emitters with emission bands at 470 and 485 nm, respectively.[3,4] However, these materials are unstable for long periods, and the purity of the color is not good enough for use in EL devices.

Quite recently, we have reported 3,4,6-triphenyl-α-pyrone derivatives (**3a**−**d**) (Scheme 1) as novel functional fluorophores for applications in EL devices as well as fluorescent pigments.[5] These compounds exhibit intense fluorescence from blue to orange in the solid state, but this fluorescence is quite weak in solution. Among these, **3a** gives quite intense emission around 470 nm (blue) which is at least three times stronger than that of Alq_3. To investigate the reason for this, we have carried out the electronic characterization of the above pyrone derivatives, particularly **3a**, from the standpoint of molecular and crystal structures as well as intermolecular interactions.

2. Experimental Section

2.1. Outline of the Synthesis. The synthetic procedure for compounds **3a**−**d** is outlined in Scheme 1. The α-pyrone derivatives were synthesized by the reaction of 4-substituted phenacyl sulfonium ylide **1** with 2,3-diphenylcyclopropenone **2**. The sulfonium ylides were prepared in situ from the corresponding sulfonium salts in the presence of base. Details of the synthesis are given elsewhere.[5]

SCHEME 1: Synthesis of 3,4,6-triphenyl-α-pyrone Derivatives.

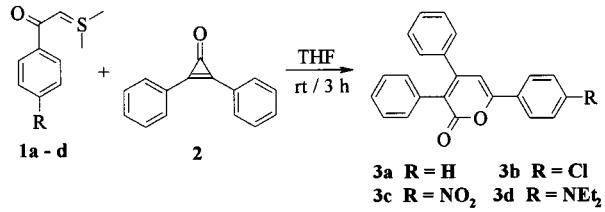

2.2. Single Crystals and Their Structure Analyses. The single crystals of compounds **3a**, **3c**, and **3d** were grown by recrystallization from solution in hexane and ethyl acetate. Reflection data were collected with an AFC5R diffractometer or RAXIS−RAPID imaging plate from Rigaku Denki. All structures were solved by direct methods.

2.3. Measurements. UV−vis absorption and fluorescent spectra were recorded on a Hitachi U-3300 spectrometer and a Hitachi F4500 fluorescent spectrometer, respectively. Polarized reflection spectra were measured on single crystals by means of a microscope−spectrophotometer (UMSP80; Carl Zeiss).

2.4. Molecular Orbital (MO) Calculations. The geometry was optimized for compounds **3a**−**d** by means of the AM1 Hamiltonian in MOPAC 93.[6] The INDO/S program used for spectroscopic calculations is part of the ZINDO program package.[7] Optical absorption bands were computed on the optimized geometry using the INDO/S Hamiltonian, and 145 configurations were considered for the configuration interaction (CI). All calculations were performed on a Power Macintosh 8500/120 computer.

10.1021/jp013850p CCC: $22.00
Published on Web 04/19/2002

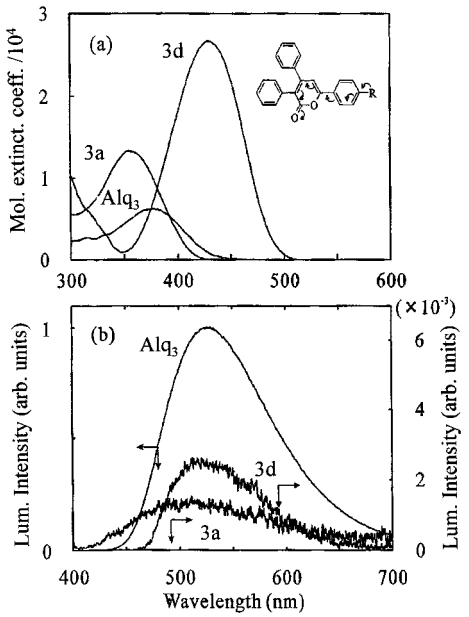

Figure 1. (a) Absorption spectra in EtOH solution for **3a**, **3d**, and Alq_3 and (b) luminescence spectra in solution for **3a**, **3d**, and Alq_3 (1 mM in toluene).

3. Results and Discussion

3.1. Absorption and Fluorescence Spectra in Solution. Figure 1a shows the solution spectra in ethanol for **3a**, **3d**, and Alq_3. The spectral shape of **3b** (λ_{max} = 358 nm; $\epsilon = 1.59 \times 10^4$ cm^{-1}) and **3c** (λ_{max} = 370 nm; $\epsilon = 1.42 \times 10^4$ cm^{-1}) is exactly the same as that of **3a**. The absorption bands of **3a**−**d** appear in the wavelength region from 350 to 425 nm, depending on the electron-donating or electron-accepting ability of the substituent R shown in the inset of Figure 1. When R is electron-donating, the chromophore forms a typical push−pull system composed of R (donor) and the oxygen atom (acceptor). This facilitates an electron transfer from donor to acceptor, so that the electron can freely move back and forth within the chromophore, leading to bathochromic shifts. The push−pull system is most effective with R = NEt_2 in **3d**, showing an extremely large bathochromic shift (λ_{max} = 425 nm). This trend is in good agreement with the results of MO calculations as described below.

Figure 1b shows the fluorescence spectra for **3a**, **3d**, and Alq_3 in solution (1 mM in toluene) where the intensity is normalized to that of Alq_3. Compound **3b** shows approximately the same intensity at nearly the same wavelength as that of **3a**; whereas no luminescence was observed for **3c**. It should be noted that the luminescence of **3a**−**d** is much weaker than that of Alq_3 by about 2−3 orders of magnitude. However, **3a**−**d** exhibit intense luminescence in the solid state as will be shown later. The emission of these compounds in other nonpolar, polar, or aprotic solvents including acetonitrile, dichloromethane, toluene, THF, and acetone are quite weak, as compared to that in the solid state. The intensity of emission of **3a** in ethanol at 50 °C was also quite weak. Therefore, the weak fluorescence in ethanol is not considered to be caused by quenching via hydrogen bonding.

3.2. Geometry Optimization and Calculated Absorption Bands. Table 1 shows the dipole moments as well as the torsion angles between the pyrone ring and the 6-phenyl group for the optimized geometries of **3a**−**d**. The calculated absorption bands and their oscillator strengths are also shown together with the experimental values in ethanol. All absorption bands are assigned to the HOMO/LUMO $\pi-\pi^*$ transition, where HOMO and LUMO denote the highest occupied molecular orbital and the lowest unoccupied molecular orbital, respectively. The transition dipole of **3a** points the direction as shown in Figure 2.

TABLE 1: Geometry Optimization and Calculated Absorption Bands for 3a−3d

compounds	dipole moment (*D*)	torsion[a] angle (deg)	cal. λ (nm)	cal. f[b]	obs. λ (nm)	obs. log ϵ[c]
3a	4.5	22.7	365.2	0.699	356	1.26
3b	4.4	22.7	365.8	0.708	358	1.59
3c	7.6	22.6	376.1	0.826	378	1.42
3d	5.3	19.3	377.5	0.841	425	2.60

[a] Torsion angle between the pyrone and 6-phenyl rings. [b] Oscillator strength. [c] Molar extinction coefficient.

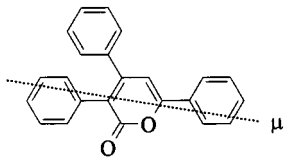

Figure 2. Direction of dipole moment of **3a**

TABLE 2: Crystallographic Data 3a, 3c, and 3d

	3a	**3c**	**3d**
R	H	NO_2	NEt_2
molecular formula	$C_{23}H_{16}O_2$	$C_{23}H_{15}O_2N$	$C_{27}H_{25}O_2N$
formula weight	324.38	369.38	395.50
color	yellow	yellow	orange
crystal shape	prismatic	block	platelet
crystal system	orthorhombic	monoclinic	monoclinic
space group	*Pbca*	$P2_1/c$	$P2_1/c$
a (Å)	18.267	16.095	10.091
b (Å)	20.298	7.308	19.522
c (Å)	8.975	16.445	11.979
β (°)		109.375	111.523
V (Å^3)	3327	1824.7	2195.28
Z	8	4	4
R-factor	0.059	0.045	0.062
torsion angle (°)[a]	25.9	18.4	8.1
dipole moment[b]	4.5	7.5	5.3

[a] Torsion angle between the pyrone and 6-phenyl rings. [b] Calculated by *MOPAC 93*.

The torsion angles between the pyrone plane and the 6-phenyl group of **3a**−**c** are around 22.7° whereas **3d** exhibits an appreciably smaller angle of 19.3°. The smaller torsion angle in turn increases the π-conjugation between the pyrone ring and the 6-phenyl group, leading to a bathochromic shift.[8] The calculated absorption bands are in semiquantitatively good agreement with the experiment, although the value for **3d** is considerably underestimated.

3.3. Crystal Structures. The crystallographic data for **3a**, **3c**, and **3d** are given in Table 2 together with the torsion angles and dipole moments. Compounds **3c** and **3d** belong to the same crystal system (monoclinic) and the same space group ($P2_1/c$). On the other hand, **3a** has higher symmetry (orthorhombic, *Pbca*).

Figure 3a shows the ORTEP plot of **3a**. The phenyl rings attached to the 3- and 4-positions of the pyrone ring are twisted, in both cases, out of the pyrone plane by about 53°, and this is also the case in **3c** and **3d**. On the other hand, as shown in Table 2, the torsion angle between the pyrone ring and 6-phenyl ring varies depending on the substituent R.

Figure 3b shows the projection of the crystal structure onto the (*b*,*c*) plane. The molecules are arranged pairwise so as to

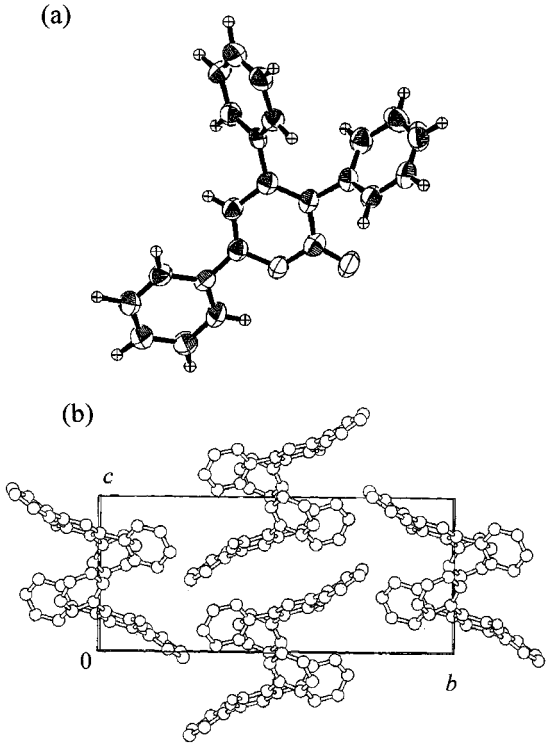

Figure 3. (a) ORTEP plot for **3a** and (b) projection of the crystal structure onto the (100) plane.

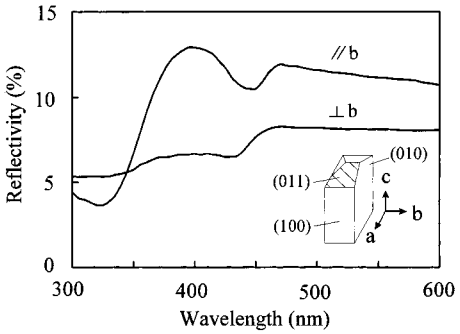

Figure 4. Polarized reflection spectra of **3a** measured on the (100) plane of single crystals. For the (100) projection, see Figure 3b.

reduce the electrostatic energy due to the dipole moment and are stacked in a herringbone fashion along the *c*-axis. This is specific to compound **3a**; no corresponding asymmetrical unit is found in **3c** and **3d**.

It is also interesting to note the difference in torsion angle between the molecule in the free space (Table 1) and the one in the lattice (Table 2). The difference in torsion angle increases in **3a** (22.7/25.9°) in the crystal while it decreases in **3c** (22.6/18.4°), but the extent is relatively small in both cases. On the other hand, the angle is remarkably reduced in **3d** from 19.3° to 8.1°. This is attributable to stronger intermolecular interactions in the solid state as compared with those in **3a** and **3c**.

3.4. Polarized Reflection Spectra of 3a. Figure 4 shows the polarized reflection spectra measured on the (100) plane of single crystals of **3a** by means of a microscope−spectrophotometer. The (100) projection is shown in Figure 3b. A prominent reflection band appears around 390 nm for polarization parallel to the *b*-axis. This reflection maximum is shifted toward longer wavelengths as compared with that of the absorption band in solution by about 36 nm (about 2933 cm^{-1}) (Figure 1). On the other hand, the reflection intensity of the same band is greatly diminished for polarization perpendicular

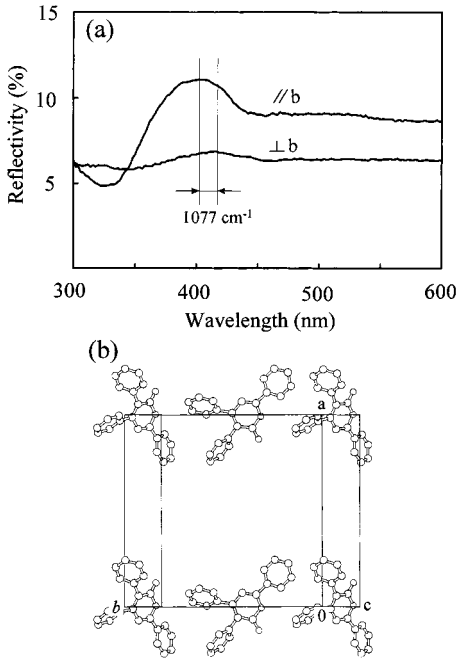

Figure 5. (a) Polarized reflection spectra of **3a** measured on the (011) plane of single crystals and (b) projection of the crystal structure onto the (011) plane.

to the *b*-axis. Since the transition dipole lies along the long molecular axis as shown in Figure 2, the polarization parallel to the *b*-axis induces considerable reflection because of the nearly head-to-tail arrangement of the transition dipoles.[9] On the other hand, the dispersion is relatively weak with polarized light along the *c*-axis (nearly ⊥*b*). This is due to the smaller projection of the transition dipole on the *c*-axis. Also observed are the monotonic reflections above 450 nm for both polarizations. This is due to the reflection from the rear (−100) plane of the single crystal and has nothing to do with the real band.

Polarization measurements were also made on the nearly-molecular plane in order to study the interaction between transition dipoles arranged in an oblique fashion. Figure 5 shows the polarized reflection spectra measured on the (011) plane (Figure 5a), together with its projection (Figure 5b). The reflection maxima appear around 390 and 418 nm for polarization parallel and perpendicular, respectively, to the *b*-axis (//*a*). The difference in reflection maxima for different polarizations amounts to about 1077 cm^{-1} and is called the Davydov splitting, which is caused by excitonic interactions between translationally inequivalent molecules.[9] The existence of Davydov splitting serves as evidence of short-range coherence of exciton packets and acquires an extended significance. This means that exciton coupling is also occurring between translationally equivalent molecules. Consequently, both effects are superimposed in such a way as to give rise to the polarized reflection spectra shown in Figure 5.

On the basis of the above discussion, the bathochromic shift (about 36 nm; 2933 cm^{-1}) on going from solution to the solid state can mainly be ascribed to the excitonic interactions in the solid state.

3.5. Luminescence in the Solid State. Figure 6 shows the fluorescent spectra in powders for **3a**, **3d**, and Alq_3, where the intensity of Alq_3 is set to 1 and is used as the reference. The luminescence for **3b** and **3c** in powders is as follows: λ_{max} = 478 nm with intensity of 1.3 for **3b** and λ_{max} = 537 nm with intensity of 0.1 for **3c**. It is remarkable to note that compounds **3a**−**d** exhibit strong luminescence in the solid state, in clear

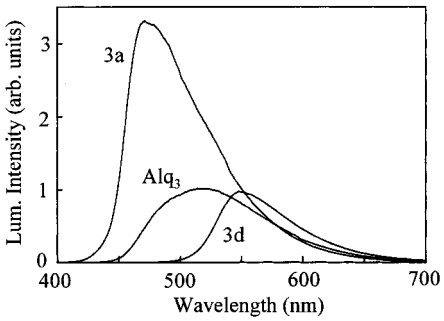

Figure 6. Luminescence spectra in powders for **3a**, **3d**, and Alq_3.

contrast to the extraordinarily weak luminescence in solution as shown in Figure 1b. Particularly, **3a** exhibits an intense blue luminescence peaking around 470 nm, and the intensity is at least three times stronger than that of Alq_3. In addition, the bandwidth of **3a** is much narrower than that of Alq_3, showing a high purity blue emission. This strongly suggests that the remarkably intense luminescence of **3a** may be applied to a blue emitter for EL devices.

The luminescence of all pyrone derivatives are greatly enhanced on going from solution to the solid state. The appearance of the luminescence is obviously due to intermolecular interactions in the solid state. Another interesting point is why the luminescence of **3a** is uniquely more intense in the solid state. In **3a**, molecules are paired up in the solid state (Figure 3b). The other crystal properties (for example, crystal system and space group) are, however, more or less the same for all pyrone derivatives. Interestingly, a quite similar luminescence enhancement has already been reported in crystal modification III of dithioketopyrropyrrole, in which the two crystallographically independent molecules are pairwise arranged in the solid state.[10] Full details of the enhancement mechanism are still not yet fully understood at the moment.

4. Conclusions

Luminescent and electronic properties of pyrone derivatives have been investigated from the standpoint of molecular and crystal structures as well as intermolecular interactions. The following conclusions can be drawn from the present investigation.

1. All pyrone derivatives exhibit an intense luminescence in the solid-state comparable with that of Alq_3, although these fluoresce extraordinarily weakly in solution. The present luminescence enhancement is obviously brought about by intermolecular interactions.

2. The blue emission of **3a** (around 470 nm) is at least three times stronger than that of Alq_3 and is characterized by a narrow emission band (i.e., high color purity). This suggests that **3a** may be a promising candidate for a blue emitter for EL devices.

3. The absorption band of **3a** is shifted toward longer wavelengths by about 36 nm (about 2993 cm^{-1}) on going from solution to the solid state. This is mainly due to excitonic interactions in the solid state.

4. The high emission efficiency of **3a** can be correlated with the pairing of two molecules, but this has yet to be confirmed.

References and Notes

(1) Tang, C. W.; Van Slyke, S. A. *Appl. Phys. Lett.* **1987**, *51*, 913.

(2) Araki, K.; Mutai, K.; Shigematsu, Y.; Yamada, M.; Nakajima, T.; Kuroda, S.;

(3) Shimano, I. *J. Chem. Soc., Perkin Trans. 2*, **1996**, 613.

(4) Tao, X. T.; Suzuki, H.; Wada, T.; Miyata, S.; Sasabe, H. *J. Am. Chem. Soc.* **1999**, *121*, 9447.

(5) Leung, L. M.; Lo, W. Y.; So, S. K.; Lee, K. M.; Choi, W. K. *J. Am. Chem. Soc.* **2000**, *122*, 5640.

(6) Hirano, K.; Minakata, S.; Komatsu, M. *Chem. Lett.* **2001**, 8.

(7) Stewart, J. J. P. *MOPAC*, ver. 93; Fujitsu, Tokyo.

(8) Zerner, M. C. *ZINDO: A General Semiempirical Program Package*; Department of Chemistry, University of Florida: Gainesville, FL, 1996.

(9) However, one of reviewers pointed out that MOPAC-calculated optimized geometry of **3a** showed quite good correlation to the results from X-ray analysis. Although **3d** showed relatively large difference in calculated and experimental torsion angles, the tendency was in good accordance with those obtained from X-ray analyses. Therefore, we used these calculated data.

(10) Craig, D. P.; Walmsley, S. H. *Excitons in Molecular Crystals*; W. A. Benjamin: New York, 1968.

(11) Mizuguchi, J.; Rochat, A. C.; Rihs, G. *Ber. Bunsen-Ges. Phys. Chem.* **1992**, *96*, 607.